Geoderma 443 (2024) 116811

Contents lists available at ScienceDirect

Geoderma

journal homepage: www.elsevier.com/locate/geoderma

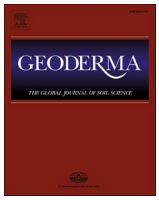

Decoding the rhizodeposit-derived carbon's journey into soil organic matter

Pedro P.C. Teixeira [a,b,*], Alix Vidal [c], Ana P.M. Teixeira [d], Ivan F. Souza [a], Luís C.C. Hurtarte [e,f], Danilo H.S. Silva [a], Luís F.J. Almeida [a], Franz Buegger [g], Edith C. Hammer [h], Jan Jansa [i], Carsten W. Mueller [j,k], Ivo R. Silva [a]

[a] Departamento de Solos, Universidade Federal de Viçosa (UFV), Viçosa, Brazil
[b] Chair of Soil Science, TUM School of Life Sciences, Technical University of Munich (TUM), Freising-Weihenstephan, Germany
[c] Soil Biology Group, Department of Environmental Sciences, Wageningen University, Wageningen, The Netherlands
[d] Departamento de Engenharia Florestal, Universidade Federal de Viçosa (UFV), Viçosa, Brazil
[e] Diamond Light Source Ltd., Oxfordshire, United Kingdom
[f] European Synchrotron Radiation Facility, Grenoble, France
[g] Research Unit Environmental Simulation, Helmholtz Zentrum München, German Research Center for Environmental Health, Neuherberg, Germany
[h] Department of Biology and Center for Environmental Sciences, Lund University, Sweden
[i] Laboratory of Fungal Biology, Institute of Microbiology, Czech Academy of Sciences, Praha, Czech Republic
[j] Department of Geosciences and Natural Resource Management, University of Copenhagen, Copenhagen, Denmark
[k] Institute of Ecology, Chair of Soil Science, Technische Universität Berlin, Berlin, Germany

ARTICLE INFO

Handling Editor: Daniel Said-Pullicino

Keywords:
Net rhizodeposition
^{13}C pulse labeling
Tropical soils
Eucalypt
Rhizosphere
Mineral-associated organic matter (MAOM)
Phospholipid fatty acids
Short-range order minerals
Metal-organic complexes

ABSTRACT

Net rhizodeposition corresponds to the portion of living root carbon (C) that remains in the soil after microbial processing and partial decomposition. Although it is assumed that this C input exerts an important role in the formation of soil organic matter (SOM), its contribution to distinct SOM pools is still not fully understood. In this study, we aimed to (i) quantify the retention of net rhizodeposition C in the different SOM fractions and in reactive Al and Fe mineral phases and (ii) investigate how rhizodeposition drives the spatial distribution of microbial communities in the rhizosphere. To track the transfer of net rhizodeposition into the soil, we used artificially labeled eucalypt (*Eucalyptus* spp.) seedlings under a ^{13}C-CO_2 atmosphere (multiple-pulse labeling). Combining physical SOM fractionation and the chemical extraction of aluminum (Al) and iron (Fe) reactive phases, we studied the distribution of net rhizodeposition into different soil fractions. We also assessed the ^{13}C incorporation into microbial phospholipid fatty acids (PLFAs) at different distances from the roots. Our results show that 76 % of the net rhizodeposition ^{13}C was retained within the mineral-associated organic matter (MAOM) fraction. About 28 % of net rhizodeposition ^{13}C within the MAOM fraction was retained within the Al and Fe reactive phases, indicating that this is a sizeable mechanism for the retention of net rhizodeposition in soil. Rhizodeposition increased the abundance of microbial PLFAs exclusively in the soil close to the roots (0–4 mm), with prominent incorporation of net rhizodeposition ^{13}C into fungal biomarkers. Overall, our findings underscore the importance of mineral associations for the retention of net rhizodeposition in the soil. We also highlight the role of fungi in transferring the root-derived C beyond the root vicinity and promoting the formation of occluded SOM.

1. Introduction

Rhizodeposition, i.e., the process of release of root-derived carbon (C)as exudates, mucilage or sloughed-off cells into the soil, represents a substantial proportion (7–11 %) of the carbon (C) flux from plants into the soil (Hinsinger et al., 2009; Jones et al., 2009; Pausch and Kuzyakov, 2018). Presumably, the vast majority of rhizodeposit C returns to the atmosphere after a few hours or days via microbial mineralization, and only a minor fraction of the rhizodeposit C persists in the soil for a longer time (Pausch and Kuzyakov, 2018). This portion of rhizodeposit C that

* Corresponding author at: Departamento de Solos, Universidade Federal de Viçosa (UFV), Viçosa, Brazil.
E-mail address: pedro.paulo.teixeira@tum.de (P.P.C. Teixeira).

https://doi.org/10.1016/j.geoderma.2024.116811
Received 9 October 2023; Received in revised form 27 January 2024; Accepted 1 February 2024
Available online 26 February 2024

persists in soil C pools either via its direct transfer and/or following microbial assimilation is defined as net rhizodeposition (Pausch and Kuzyakov, 2018). Recent evidence points that net rhizodeposition contributes significantly to the formation of persistent soil organic matter (SOM) (Cotrufo et al., 2013; Sokol et al., 2018; Villarino et al., 2021). Nevertheless, the mechanisms responsible for converting it into SOM are still poorly understood (Kögel-Knabner, 2017).

The persistence of SOM in the soil is attributed to two main mechanisms: (i) spatial inaccessibility, provided by the occlusion in aggregates (Angst et al., 2017; Baumert et al., 2021, 2018), and (ii) interaction with mineral surfaces and metal ions through the formation of mineral-organic associations (Sokol et al., 2018; von Lützow et al., 2006). The interaction with the mineral matrix is assumed to be dominant in the preservation of net rhizodeposition (Sokol et al., 2018; Villarino et al., 2021), although it is complicated to evaluate the relative importance of each mechanism separately. One possible way to disentangle the importance of these two mechanisms responsible for the retention of net rhizodeposits in the soil is to use physical SOM fractionation according to particle size and density. Separating SOM into distinct fractions is a widely used technique that can provide a quantitative description of the mechanisms responsible for the retention of rhizodeposits in the soil (Angst et al., 2023; von Lützow et al., 2007; Witzgall et al., 2021).

Among the components of the mineral matrix, reactive phases of aluminum (Al) and iron (Fe) are well-known as important agents for the formation of mineral-organic associations (Kleber et al., 2005; Mikutta et al., 2006). The retention of organic compounds by such minerals is often linked to their large specific surface area coupled with the presence of abundant reactive sites suitable for adsorption reactions (Kaiser and Guggenberger, 2003) and the capacity of these minerals to entrap organic compounds through co-precipitation (Kleber et al., 2015; Mikutta et al., 2011). These minerals can retain large amounts of C even when present in low quantities compared to other more crystalline phases (Porras et al., 2017; Souza et al., 2017).

The release of rhizodeposits into the soil leads to the formation of a C concentration gradient from the roots to the surrounding soil, which affects the abundance and composition of the soil microbial communities (Kuzyakov and Razavi, 2019; Paterson et al., 2007). The high concentration of C in the vicinity of the roots may provide favorable conditions for the microorganisms with low motility that mainly rely on the use of easily available forms of C, such as bacteria (Gunina et al., 2014; Ingwersen et al., 2008; Poll et al., 2006). In contrast, fungal hyphae can expand beyond the roots, acting as conduits for transferring rhizodeposit-C toward more distant regions of the non-rhizospheric soil (Johnson et al., 2002; Vidal et al., 2021). Gaining insights into microbial spatial gradients is essential to improve our understanding of fate of rhizodeposits in the soil.

The goals of this study were to (i) quantify the retention of net rhizodeposition C in the different SOM fractions (free, occluded and mineral-associated SOM) and in reactive Al and Fe mineral phases and (ii) investigate the effects of rhizodeposition on the spatial distribution of microbial communities. To this end, we employed a multiple pulse ^{13}C labeling approach to track the transfer of rhizodeposit C from eucalypt seedlings (*Eucalyptus* spp.) along the root-to-soil gradient. We predict that: (i) the retention of net rhizodeposition C is primarily driven by its interaction with mineral matrix, with predominant incorporation into reactive phases of Al and Fe, and (ii) the effects of rhizodeposition on the microbial community will be restricted to the vicinity of the roots, with preferential incorporation of rhizodeposits into bacterial communities.

2. Material and methods

2.1. Soil characteristics

The soil was sampled from the 0–20 cm layer of a eucalypt plantation in São Sebastião da Vargem Alegre – Brazil (21°01′37″ S 42°34′12″ W) and was classified as a Rhodic Ferralsol (IUSS Working Group WRB, 2022 – Fig. S1). The fresh sampled soil was sieved through a 2.0 mm sieve, homogenized, and plant (macro) residues were manually removed. The soil had the following physicochemical attributes: pH of 4.0 (H_2O); C and N contents of 32.2 g kg^{-1}, $\delta^{13}C$ of −23.0 ‰, and 1.9 g kg^{-1}, respectively; and clay, silt, and sand contents of 66 %, 9 %, and 25 %, respectively. Additional biogeochemical soil characteristics are shown in Table S1. Before establishing the eucalypt plantation, the site was used as pasture with the C4 tropical grass (*Urochloa decumbens*).

2.2. Experimental setup

We set up our experimental units by preparing 16 mesocosms (2.5 L plastic pots) filled with the soil material described above. Further, we also prepared four ingrowth cores to be placed within each mesocosm; hence, we had a total of 64 cores. We set up these ingrowth cores by packing the soil inside aluminum cylinders (height 2.5 cm, diameter 4.7 cm) at a density of 1.13 g cm^{-3} (adapted from Shahzad et al., 2015). To restrict the root growth inside the cores but to allow the movement of water, nutrients, microorganisms, and rhizodeposits, the cores were capped at one side with a nylon mesh membrane of 5.0 μm pore size (Tegape, Curitiba, Brazil) and sealed at the other side. This was done to create a rhizospheric gradient in the soil inside the ingrowth cores.

Within each mesocosm, four ingrowth cores were placed horizontally with a mesh side towards the rooting zone of the seedling. (Fig. S1). We set two treatments: with rhizodeposition, which had an actively growing eucalypt seedling (*Eucalyptus grandis* x *E. urophylla* - I144), and control, which was left unplanted (Fig. 1). The seedlings used in this study had a similar size and phenological characteristics (four fully expanded leaf pairs). In both treatments, a nutrient solution was mixed in the soil to provide nutrients before the mesocosm assembly, according to specific requirements of eucalypt cultivation in pot experiments (Novais et al., 1991 – Table S2). This procedure was done to ensure optimal development of the eucalypt plants by minimizing nutrient limitations. The soil had a water holding capacity (WHC) of 33 %, and the mesocosms were irrigated daily with deionized water to maintain moisture between 60 and 80 % of the soil water holding capacity (evaluated by weighting the mesocosms). The experiment was conducted in a randomized block design in an open greenhouse with 4 replicates.

2.3. ^{13}C labeling and unlabeled references

During the experiment, half of the mesocosms were ^{13}C labeled (four mesocosms with plants and four without plants) using a multiple-pulse labeling approach (adapted from Machado et al., 2011). The remaining half (eight) of the mesocosms were kept as unlabeled references for isotopic calculations. We started the ^{13}C labeling 15 days after planting the seedlings, and in total, we performed 10 labeling events (Fig. 1). In each labeling event, the mesocosms were placed randomly inside a labeling glass chamber (448.0 dm^3) for 10 h and submitted to a ^{13}C-CO_2 enriched atmosphere (Fig. S2). We applied the first four labeling events once per week, with one pulse per day. The remaining labeling events (5^{th} to 10^{th}) were applied twice a week with two pulses per labeling event (one pulse in the morning and another in the afternoon, each one lasting 5 h). The ^{13}C-CO_2 enriched atmosphere was generated by injecting 20 mL of a 1 M H_2SO_4 solution through a septum into a petri-dish located inside the chamber containing 1.0 g of $Na_2^{13}CO_3$ (99 atom %). In total, 1.85 g of ^{13}C was added during the labeling, which is equivalent to 0.46 g of ^{13}C per plant.

The remaining half of the mesocosms were kept as unlabeled references for isotopic calculations. These mesocosms had the same treatments (planted and control) and were subject to the same procedure described for labeled mesocosms. In contrast to the labeled mesocosms, the pulses were done using a non-isotopically enriched Na_2CO_3 analog (Fig. 1). Thus, the overall CO_2 concentration would have been similar for

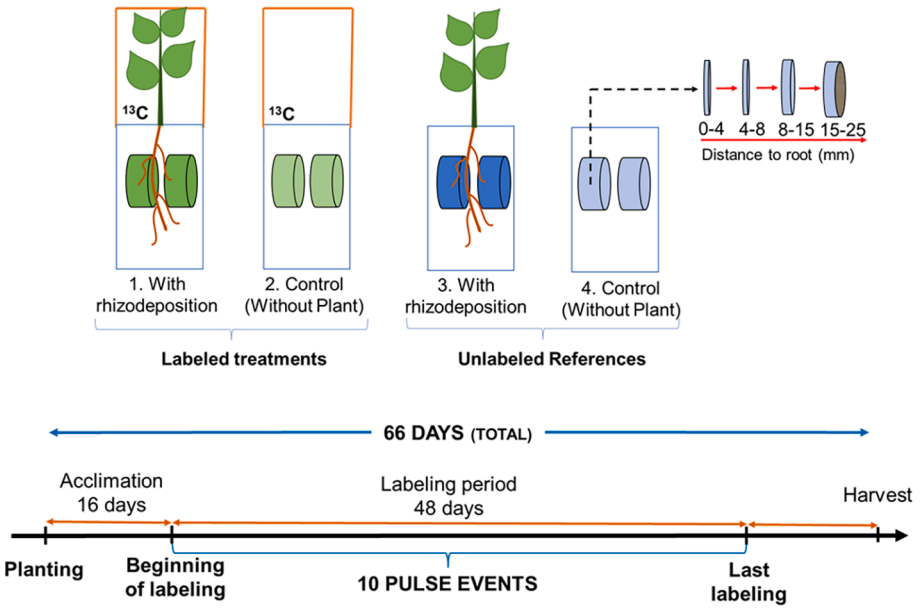

Fig. 1. Simplified representation of the experimental design and the soil slicing, and a timeline of the experiment presenting the timing of labeling events. For simplification purposes, only two (not four) root ingrowth cores are represented in each mesocosm.

both groups of treatments, despite their differential ^{13}C labeling. During each labeling procedure (labeled and unlabeled references), the temperature was recorded, and the concentration of ^{12}C-CO_2 and ^{13}C-CO_2 inside the chamber were measured over time with a cavity ring-down spectrometer (CRDS, Picarro, Sunnyvale, United States of America – Table S3).

2.4. Sampling

To ensure the formation of the rhizosphere within the ingrowth cores, the development of the root system was monitored through destructive sampling of additional experimental unities that were grown in the same conditions as the plants of our study. The formation of a substantial root mat in the vicinity of the mesh of the cores was observed 66 days after planting (Fig. S3), indicating that the mesocosms were ready for sampling. After the sampling of the plants (Table S4), one of the cores (out of four) per mesocosms was collected and sliced into four layers: 0–4, 4–8, 8–15, and 15–25 mm (distance to the root – Fig. 1). The sectioning of the layers was done with an adapted holding device pushing the soil layer out of the cores and progressively cutting the layers manually with a razor blade. A subset of approximately 3.0 g of each layer of soil was freeze-dried for phospholipid fatty acid (PLFA) analysis, and the remaining soil was air-dried and sieved at 2.0 mm. The three remaining ingrowth cores were separated to be used in another experiment and are not part of this study.

2.5. SOM fractionation

To quantify the distribution of net rhizodeposition ^{13}C in different SOM fractions, soil samples from the 0–4 mm layer were fractionated according to a combined density and particle size fractionation adapted from Mueller and Koegel-Knabner (2009). For this analysis, only samples from the 0–4 mm layer were selected because of their proximity to the roots and their higher ^{13}C enrichment. Briefly, 3.0 g of air-dried soil was gently saturated with 40.0 mL of sodium polytungstate (SPT) solution (density of 1.8 g cm^{-3}) and left overnight. Subsequently, the floating free particulate organic matter (fPOM) was collected with suction using a vacuum pump. The remaining suspension was ultrasonicated with an energy input of 460.0 J mL^{-1} (Carolino de Sá et al., 1999) to release the occluded particulate organic matter (oPOM), which was collected with vacuum pump after centrifugation (2744 g for 30 min). The fPOM and oPOM fractions were rinsed with deionized water using a pressure filtration system (0.22 µm pore nylon filter – Berrytec, Grünwald, Germany) until the electrical conductivity was below 2.0 µS cm^{-1} to remove excessive salt from the above fractions and thus allow quantification of C and N in the POM fraction (Angst et al., 2016). The remaining mineral residue was washed with deionized water until the electrical conductivity was below 50.0 µS cm^{-1} (Angst et al., 2016). To avoid the loss of mineral particles, the water used to wash the mineral fraction was collected and rinsed in a pressure filtration system like the fPOM and oPOM fractions. After the removal of salts, the mineral residues retained on the filter were combined with the remaining mineral residues and sieved through a 63.0 µm mesh sieve using deionized water to obtain the fractions smaller than 63.0 µm (henceforth referred to as mineral-associated organic matter - MAOM) and larger than 63.0 µm (sand-sized organic matter - SSOM). The mean recovery of the SOM fractionation for C and N was 92 % and 89 %, respectively. The excessive water volume in the suspensions of all fractions was first reduced in an oven at 40 °C, and subsequently, all fractions were freeze-dried.

2.6. Sequential extraction of Al and Fe reactive phases

We evaluated the retention of net rhizodeposition ^{13}C on the Al and Fe reactive phases using the sequential extraction adapted from Heckman et al. (2018). Using 1.0 g of the MAOM fraction from the 0–4 mm layer, we first extracted the metal–organic complexes (MOC) with sodium pyrophosphate and then the short-range order (SRO) phases using hydroxylamine. Both extracts were shaken for 16 h (at 300 RPM) in the dark and centrifuged (2744 g) for 1 h. The supernatants were filtered through 0.2 µm polyethersulfone syringe filters (Phenomenex Ltd, Aschaffenburg, Germany). The residual soil was oven-dried at 40 °C, ground, homogenized, and subsampled before the next extraction. Concentrations of Al and Fe in the extracts were determined using an inductively coupled plasma-optic emission spectrometer (ICP-OES) (Vista-Pro CCD simultaneous, Varian, Darmstadt, Germany). The C contents were measured in a subsample of the residual soil after each extraction step (see item 2.7). The amount of C extracted at each step was calculated by determining the difference between consecutive steps of the sequential extraction (solid-phase approach - Heckman et al., 2018).

Table 1
Total organic carbon (C) and total nitrogen (N) contents, and C/N ratios of the treatments with rhizodeposition and control along with the distances to the root (mm).

	Treatment	Distance to the root			
		0–4 mm	4–8 mm	8–15 mm	15–25 mm
C (mg g^{-1})	With rhizodeposition	32.2 ± 0.5 **a**[1]	34.1 ± 0.7 **a**	33.0 ± 0.2 **a**	32.5 ± 0.4 **a**
	Control	33.1 ± 0.4 **a**	33.3 ± 0.4 **a**	33.0 ± 0.3 **a**	31.9 ± 0.8 **a**
N (mg g^{-1})	With rhizodeposition	2.1 ± 0.1 **b**	2.3 ± 0.1 **a**	2.2 ± 0.1 **a**	2.2 ± 0.1 **a**
	Control	2.3 ± 0.1 **a**	2.3 ± 0.1 **a**	2.2 ± 0.1 **a**	2.2 ± 0.1 **a**
C/N	With rhizodeposition	15.1 ± 0.1 **a**	15.2 ± 0.1 **a**	15.0 ± 0.1 **a**	15.0 ± 0.1 **a**
	Control	14.5 ± 0.1 **b**	14.6 ± 0.1 **a**	14.7 ± 0.1 **a**	14.6 ± 0.1 **b**

[1] Different letters indicate significant differences between the treatments with rhizodeposition and control. Means ± SE (n = 4) are compared between treatments by *t*-test at 0.05 of significance.

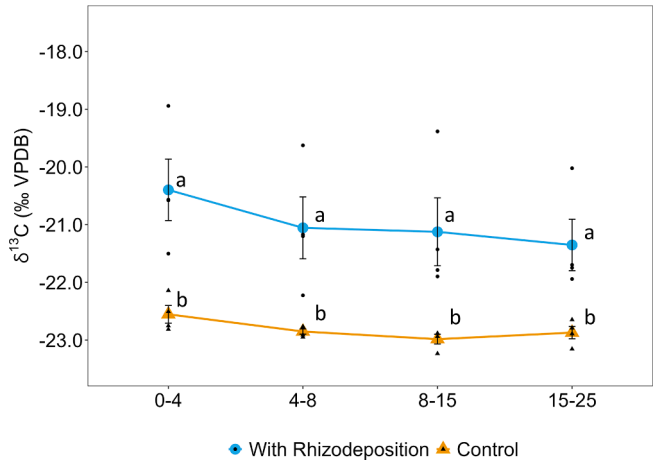

Fig. 2. Soil $\delta^{13}C$ values (‰VPDB) for the treatment with rhizodeposition and control as a function of the distance to the roots. Different letters indicate significant differences between the treatments with rhizodeposition and control. Means ± SE (n = 4) from all treatments is compared by *t*-test at 0.05 of significance.

2.7. Elemental analysis and isotopic calculations

All samples (bulk for all soil layers, SOM fractions at 0–4 mm, and the remaining soil after Al and Fe phases extractions at 0–4 mm) were analyzed for total C content and nitrogen (N) contents, and $\delta^{13}C$ using an Elemental Analyzer (Euro EA, Eurovector, Milan, Italy) coupled to an isotopic ratio mass spectrometer (IRMS delta V Advantage, Thermo Fisher, Dreieich, Germany).

The distribution of net rhizodeposition ^{13}C in each of the SOM fractions was expressed as a percentage of the total ^{13}C recovered in unfractionated soil (adapted from Hafner et al., 2012). The complete description of the calculations can be found in the supplementary material 2. In brief, the $\delta^{13}C$ (‰) values were converted to ^{13}C atom% excess, and the ^{13}C enrichment of each soil layer or SOM fraction (^{13}C atom% excess) was calculated according to the Eq. (1):

$$^{13}C\ atom\%\ excess = {}^{13}C\ atom\%\ [sample] - {}^{13}C atom\%\ [unlabeled\ control] \quad (1)$$

Where ^{13}C atom% excess is the enrichment of ^{13}C (%); ^{13}C atom% [sample] is the ^{13}C enrichment expressed as ^{13}C atom% in the samples (%), and ^{13}C atom% [unlabeled control] is the ^{13}C enrichment expressed as ^{13}C atom% in the unlabeled control. The unlabeled control comprised the unlabeled mesocosm without plants. Initially, we decided to include unlabeled references with plants in our experimental design to account for potential changes in the ^{13}C enrichment derived from the eucalypt C input in the soil. This was necessary because the soil had a $\delta^{13}C$ value of −23.0 ‰, and the eucalypt C inputs (C3 plant) could potentially reduce its ^{13}C enrichment. Nevertheless, there was no difference between the isotopic signature between the planted and unplanted unlabeled references at the end of the experiment (Table S5). In this sense, we opted to keep only the unplanted soil as unlabeled references for the ^{13}C atom% excess calculation, as it is more commonly used in the pulse labeling experiments.

The amount of ^{13}C in excess that was incorporated in each soil layer or SOM fraction (net rhizodeposition ^{13}C) was calculated according to Eq. (2):

$$\text{Net rhizodeposition } {}^{13}C = {}^{13}C\ atom\%\ excess/100 \times C\ content \times M\ 13\text{-carbon}/M\ carbon \times 1000 \quad (2)$$

Where net rhizodeposition ^{13}C is the amount of ^{13}C in excess in a given SOM fraction (μg of ^{13}C/g of soil), ^{13}C atom%excess is the enrichment of ^{13}C, C content is the content of C (mg g^{-1} of soil), *M* 13-carbon is the molar mass of ^{13}C (13.0 mg $mmol^{-1}$), *M* carbon is the molar mass of C (12.011 mg $mmol^{-1}$). The relative distribution of net rhizodeposition ^{13}C in the SOM fractions of the same experimental unit was calculated by the ratio between the net rhizodeposition ^{13}C in a given fraction and the sum of net rhizodeposition ^{13}C in all SOM fractions. This approach allowed us to quantify potential losses of ^{13}C.

2.8. PLFA analysis and calculations

The incorporation of rhizodeposition ^{13}C into the soil microbial community and the shifts in its structure were assessed by analysis of ^{13}C-enrichment in the phospholipid fatty acids (PLFA) for two selected layers of soil cores: 0–4 and 15–25 mm, and for three of the replicates. We selected these two layers because of their contrasting positions of the ingrowth core (Fig. 1), which allows the evaluation of the spatial effects in microbial communities along the root-to-soil gradient.

The extraction of PLFAs followed the methodology described by Frostegård et al. (1991) and adapted by Kramer et al. (2013). Total lipid extraction was carried out by treating 2.0 g of freeze-dried soil with Bligh & Dyer solution (methanol, chloroform, and citrate pH 4, 2:1:0.8, v/v/v) followed by solid-phase extraction on silica gel columns (0.5 g SiOH, Bond Elut, Agilent). The polar fraction was converted into fatty acid methyl esters (FAMEs) by alkaline methanolysis and the extracts were dissolved in isooctane and stored for further analysis. We measured the PLFA samples in a Trace 1300 gas chromatograph (ThermoFisher Scientific, Waltham MA, USA) equipped with a ZB-5HT column (60 m, 0.25 I.D., 0.25 μm film thickness; Phenomenex, Aschaffenburg, Germany) and flame ionization detector. The PLFA was quantified relative to an internal standard (nonadecanoic acid methyl ester – 19:0) and normalized according to the mean of results for a standard soil that was extracted along with the samples (Baumert et al., 2021, 2018). The isotopic enrichment of PLFAs was further analyzed with GC Isolink Trace GC ultra coupled to a Delta V Advantage IRMS (ThermoFisher Scientific). Unlabeled samples were also included in the analysis.

Table 2
Total carbon (C) and nitrogen (N) contents, total amounts of C and N associated with the fractions, C/N ratios, and $\delta^{13}C$ (‰VPDB) of the following SOM fractions: free-particulate organic matter (fPOM), occluded organic matter (oPOM), sand-sized organic matter (SSOM), mineral associated organic matter (MAOM)for the treatments with rhizodeposition and control at the 0–4 mm layer.

	Treatment	SOM fraction			
		fPOM	oPOM	SSOM	MAOM
C content (mg g^{-1} fraction)	With rhizodeposition	310.0 ± 24.3 **a**[1]	446.3 ± 8.6 **a**	3.4 ± 0.1 **a**	33.1 ± 0.2 **a**
	Control	325.0 ± 5.9 **a**	416.8 ± 27.1 **a**	4.1 ± 0.2 **a**	33.3 ± 0.1 **a**
N content (mg g^{-1} fraction)	With rhizodeposition	10.4 ± 0.8 **b**	18.8 ± 0.5 **a**	0.2 ± 0.1 **a**	2.4 ± 0.1 **a**
	Control	12.5 ± 0.2 **a**	17.1 ± 1.2 **a**	0.2 ± 0.1 **a**	2.3 ± 0.1 **a**
Fraction-associated C[2] (mg C g^{-1} soil)	With rhizodeposition	2.6 ± 0.6 **a**	4.8 ± 0.7 **a**	0.7 ± 0.1 **b**	25.6 ± 0.1 **a**
	Control	1.8 ± 0.5 **a**	2.4 ± 0.6 **b**	0.9 ± 0.1 **a**	25.6 ± 0.1 **a**
Fraction-associated N[2] (mg N g^{-1} soil)	With rhizodeposition	0.1 ± 0.1 **a**	0.2 ± 0.1 **a**	0.1 ± 0.1 **a**	1.8 ± 0.1 **a**
	Control	0.1 ± 0.1 **a**	0.1 ± 0.1 **b**	0.1 ± 0.1 **a**	1.8 ± 0.1 **a**
C/N	With rhizodeposition	30.7 ± 4.3 a	23.8 ± 0.6 **a**	20.6 ± 0.9 **a**	13.9 ± 0.1 **b**
	Control	26.1 ± 0.1 **b**	24.4 ± 0.4 **a**	19.5 ± 0.7 **a**	14.3 ± 0.1 **a**
$\delta^{13}C$ (‰VPDB)	With rhizodeposition	−28.0 ± 0.1 **a**	−27.8 ± 0.1 **a**	−24.6 ± 0.1 **a**	−20.0 ± 0.5 **a**
	Control	−28.7 ± 0.1**b**	−28.1 ± 0.1**b**	−24.3 ± 0.1 **a**	−22.4 ± 0.1 **b**

[1] Different letters indicate significant differences between the treatments with rhizodeposition and control. Means ± SE (n = 4) are compared between treatments by *t*-test at 0.05 of significance.
[2] The amount of fraction-associated carbon and nitrogen in each fraction was calculated from the product between its mass proportion and content.

Subsequently, the PLFAs were classified in bacteria (i15:0, a15:0, i16:0, i17:0, cy17:0, cy19:0, 15:0, 16:1ω7, and 17:0), fungi (18:1ω9, 18:2ω6,9), and unspecified microorganisms (14:0, 16:0, 18:0, 20:0) (Baumert et al., 2018). The obtained values of ^{13}C-enrichment in the individual PLFAs were calculated in a similar way as the soil samples, and it is detailed in Supplementary material 2. The relative ^{13}C-PLFA distribution in each microbial group (%) was calculated according to Eq. (3) (Zhu et al., 2017):

$$\text{Relative } ^{13}\text{C-PLFA distribution} = {}^{13}\text{C-PLFA group}/\sum {}^{13}\text{C-PLFA} \times 100 \quad (3)$$

Where ^{13}C-PLFA group is the amount of ^{13}C-PLFA incorporated into a specific microbial group, and $\sum^{13}C$-PLFA × 100 is the total amount ^{13}C-PLFA incorporated into soil microorganisms (Total PLFA).

2.9. Statistical analysis

We assessed the impacts of rhizodeposition in soil variables using non-paired t-tests (With Rhizodeposition *vs.* Control). The homogeneity of variance was checked by Levene test, and the Shapiro-Wilk test was performed to test the normal distribution of the data. When required, data transformation was performed. All statistical analysis was conducted in R v. 4.1.2 (R Core Team, 2022; RStudio, 2023). The packages *tidyverse* (Wickham et al., 2019), *car* (Fox and Weisberg, 2019), and *ggplot2* (Wickham, 2016) were used for data processing, statistical analysis, and plotting the graph, respectively. We set the probability level of significance at $p < 0.05$.

3. Results

3.1. Total soil carbon and nitrogen contents, and $\delta^{13}C$ values

Rhizodeposition did not affect total soil C content at any distance from the root (mean of all distances 32.9 ± 0.2 mg g^{-1} – Table 1). We observed a 6 % reduction of the total N content in the 0–4 mm layer in relation to the unplanted control (2.1 ± 0.1 *vs.* 2.3 ± 0.1 mg g^{-1}, respectively - Table 1). Concomitantly, an increase of 4 % and 3 % in the C/N ratio was also detected in the distances 0–4 and 15–25 mm, respectively (Table 1).

Compared with the control, the $\delta^{13}C$ values were significantly higher with rhizodeposition at all distances from the roots (Fig. 2). In this treatment, the ^{13}C enrichment tended to decrease along with root-to soil gradient, exhibiting the highest $\delta^{13}C$ values at 0–4 mm (-20.4 ‰) and the

Table 3
Iron (Fe), Aluminum (Al), and total carbon (C) bound in metal–organic (MO) complexes (Na-pyrophosphate) and short-range-order (SRO) phases of Al and Fe (Hydroxylamine) from the mineral associated fraction (MAOM) of the treatment with rhizodeposition and control at 0–4 mm layer.

	Treatment	Total[1]	MO complexes	SRO phases
Fe (mg g^{-1})	With rhizodeposition	156.2 ± 1.0	29.9 ± 1.0 **a**[2]	2.4 ± 0.1 **a**
	Control		33.5 ± 2.8 **a**	2.2 ± 0.1 **a**
Al (mg g^{-1})	With rhizodeposition	200.3 ± 1.5	21.5 ± 0.4 **a**	34.1 ± 1.2 **a**
	Control		23.4 ± 1.3 **a**	34.0 ± 1.6 **a**
C (mg g^{-1})	With rhizodeposition	33.2 ± 0.2 **a**	14.2 ± 0.6 **a**	5.8 ± 0.7 **a**
	Control	33.3 ± 0.1 **a**	14.9 ± 0.5 **a**	5.2 ± 1.0 **a**

[1] The total amount for Fe and Al was obtained from the extraction with $HClO_4/HNO_3/HF$. For C, the total value refers to the C content obtained for the MAOM fraction before the sequential extraction of Al and Fe reactive phases (also presented in Table 2).
[2] Different letters indicate significant differences between the treatments with rhizodeposition. Means ± SE (n = 4) are compared between treatments by *t*-test at 0.05 of significance.

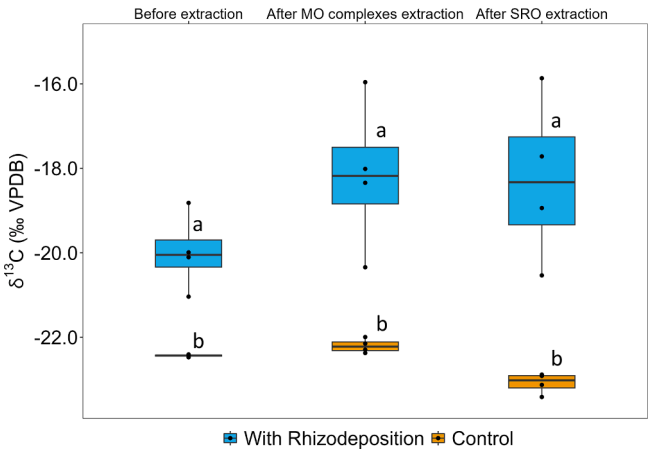

Fig. 3. $\delta^{13}C$ values (‰VPDB) in the residual mineral-associated fraction (MAOM) after the sequential extraction of Al and Fe from metal-organic complexes (MOC) and short-range order (SRO) phases for the treatment with rhizodeposition and control in the 0–4 mm layer. Means ± SE (n = 4) from all treatments is compared by *t*-test at 0.05 of significance.

lowest at 15–25 mm (-21.4 ‰). Meanwhile, the ^{13}C enrichment in controls tended to be similar along with the distance to the root, with an average of 22.8 ‰ ±0.3.

3.2. Soil organic matter fractionation

The total C and N contents in the investigated SOM fractions were not altered by the presence of rhizodeposits (Table 2), except for the total N content of the fPOM fraction, which decreased by 5 % in relation to the control ($p < 0.05$). Despite of this, we observed that rhizodeposition almost double the amount of C and N retained within the oPOM fraction ($p < 0.05$ – Table 2). Meanwhile, rhizodeposition reduced the C associated with SSOM by 20 % ($p < 0.05$ – Table 2). Rhizodeposition did not affect the amount of C and N within the MAOM fraction, but significantly decreased its C/N ratio (13.9 ± 0.1 *vs.* 14.3 ± 0.1, respectively - Table 2).

The presence of rhizodeposition significantly increased the $\delta^{13}C$ values in all fractions, except for SSOM (Table 2). In the MAOM, the $\delta^{13}C$ values increased from −22.4 ‰ to −20.0 ‰; in oPOM, increased from −28.1 ‰ to −27.8 ‰, and in fPOM increased from −28.1 ‰ to −27.8 ‰ (Table 2).

3.3. Sequential extraction of al and Fe reactive phases in MAOM fraction

The rhizodeposition did not affect the amount of Al, Fe and the total amount of C bound to the MOC and SRO phases in the MAOM fraction (Table 3). More than 40 % of the total amount of C within the MAOM fraction was extractable as MOC, while only 18 % were extractable as SRO phases. From the total amount of Fe and Al present in the MAOM fraction, 20 % and 11 % were extracted with the MOC, and 1 % and 17 % were extracted with SRO phases, respectively (Table 3).

The $\delta^{13}C$ values after the extraction of the Al and Fe phases were higher in the treatment with rhizodeposition in relation to the control ($p < 0.05$ – Fig. 3). After the extraction of MOC, the $\delta^{13}C$ values of the residual MAOM was −18.2 ‰ for the treatment with rhizodeposition and −22.2 ‰ for the control. After the extraction of SRO, the residual MAOM had a $\delta^{13}C$ value of −18.3 ‰ for the treatment with rhizodeposition and −23.1 ‰ for the control. Overall, extraction of Al and Fe phases tended to increase the difference in the ^{13}C enrichment between the treatment with rhizodeposition and the control.

3.4. Relative distribution of net rhizodeposition ^{13}C in SOM fractions

We recovered 76.2 ± 3 % of net rhizodeposition ^{13}C in the MAOM fractions (Fig. 4 and Table 5), whereas the other fractions retained much less net rhizodeposition ^{13}C, with oPOM and fPOM accounting for only 3.0 % ±1 and 2.8 % ±1, respectively. The amount of net rhizodeposition ^{13}C in SSOM was negligible. It has to be noted that 18 % of the net rhizodeposition ^{13}C was not recovered after the fractionation procedure (Fig. 4). Additionally, within the Al and Fe extracts, we observed that 11.6 % of the MAOM net rhizodeposition ^{13}C was associated with MOC, as 16.3 % was associated with SRO phases (Fig. 4). The remaining net rhizodeposition ^{13}C (75 %) stored in the MAOM fraction was not extracted with Al and Fe hydroxide sequential extraction and was found in the residual extract (Fig. 4).

3.5. PLFA and microbial communities

The abundance and characteristics of the microbial community were exclusively affected at 0–4 mm, but not at the 15–25 mm layer (Table 4). In the 0–4 mm layer, rhizodeposition increased significantly total PLFA by 80 %, bacterial biomarkers by 103 %, and fungal biomarkers by 25 %. At 15–25 mm, there was no difference between the treatment with rhizodeposition and the control in any of the parameters evaluated (Table 4). The amount of unspecified microorganism biomarkers and the

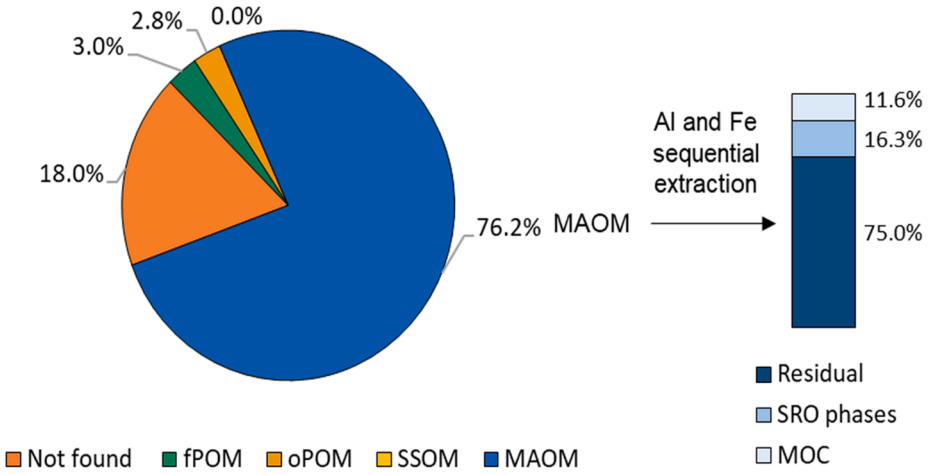

Fig. 4. Relative distribution of ^{13}C net rhizodeposition in the following SOM fractions: free-particulate organic matter (fPOM), occluded organic matter (oPOM), sand-sized organic matter (SSOM), mineral-associated organic matter (MAOM), metal–organic complexes (MOC), short-range order (SRO) phases and residual (not extracted). Means (n = 4) were calculated in relation to the unfractionated soil from the treatment *With Rhizodeposition*. A detailed version of this graph is provided in Table 5.

Table 4
Total Phospholipid fatty acids (PLFA) normalized for bulk C (nmol/g soil C), biomarkers from unspecified microorganisms, bacteria, and fungi, and fungal-to-bacterial ratio (F:B), in the treatments with rhizodeposition and control at the distances from the root of 0–4 mm and 15–25 mm.

	Treatment	Distance to root	
		0–4 mm	15–25 mm
Total PLFA (nmol g^{-1} soil C)	With Rhizodeposition	2.03 ± 0.19 **a**[1]	1.81 ± 0.12 **a**
	Control	1.32 ± 0.14 **b**	2.13 ± 0.34 **a**
Unspecified microorganisms (nmol g^{-1} soil C)	With Rhizodeposition	0.65 ± 0.06 **a**	0.55 ± 0.03 **a**
	Control	0.44 ± 0.10 **a**	0.64 ± 0.10 **a**
Bacteria (nmol g^{-1} soil C)	With Rhizodeposition	0.73 ± 0.10 **a**	0.71 ± 0.07 **a**
	Control	0.36 ± 0.07 **b**	0.97 ± 0.21 **a**
Fungi (nmol g^{-1} soil C)	With Rhizodeposition	0.66 ± 0.04 **a**	0.54 ± 0.02 **a**
	Control	0.53 ± 0.02 **b**	0.52 ± 0.03 **a**
F:B	With Rhizodeposition	0.93 ± 0.14 **a**	0.77 ± 0.12 **a**
	Control	1.55 ± 0.38 **a**	0.59 ± 0.23 **a**

[1] Different letters indicate significant differences between the treatments with rhizodeposition and control. Means ± SE (n = 3) are compared between treatments by *t*-test at 0.05 of significance.

F:B ratio was not affected by rhizodeposition in any of the layers (Table 4).

The relative ^{13}C-incorporation into PLFA assigned to different microbial groups was very similar in the different distances of the roots (0–4 mm and 15–25 mm - Fig. 5). The majority of ^{13}C-PLFA was recovered as fungal biomarkers (47–52 %), followed by unspecified microorganisms biomarkers (30–35 %). Bacterial biomarkers accounted for the smallest portion of the recovered ^{13}C-PLFA (17–19 %).

4. Discussion

4.1. From rhizodeposits to mineral-associated organic matter

More than 75 % of the net rhizodeposition ^{13}C was recovered in the MAOM fraction (Fig. 4). This finding highlights the importance of mineral-organic interactions for the retention of the rhizodeposits in the soil, as has been previously discussed by Sokol et al. (2022) and Villarino et al. (2021). Rhizodeposits are particularly rich in low molecular weight soluble compounds, which can be adsorbed into the mineral surfaces directly or after their partial decomposition by soil microorganisms (Mikutta et al., 2019; Sokol et al., 2018). The interactions with the minerals reduce/prevent the decomposition of these compounds, increasing their residence time in the soil (Cotrufo et al., 2013). Our study provides direct evidence of the conversion of rhizodeposits into the MAOM fraction, extending results obtained from pure minerals or labeled reactants that were used as proxies of rhizodeposits (Neurath et al., 2021; Sokol and Bradford, 2019; Wu et al., 2022). Nevertheless, it is important to recognize that the fraction that is operationally obtained as MAOM is not homogeneous in terms of persistence and contains a highly dynamic portion that can be further decomposed by microorganisms (Sokol et al., 2022).

Although only 2.8 % of the net rhizodeposition ^{13}C was allocated to oPOM, we observed that root activity almost doubled the C associated with oPOM fraction (Table 2). The occlusion of SOM inside aggregates represents an important mechanism for SOM protection (Dungait et al., 2012; von Lützow et al., 2008). Rhizodeposition-induced aggregation was shown to be mainly associated with the formation of macroaggregates and is mostly controlled by root growth and fungal hyphae expansion in soil (Baumert et al., 2021, 2018; Jeewani et al., 2020; Oades and Waters, 1991). An enhanced fungal activity is supported by the PLFAs results, which highlight the incorporation of rhizodeposit-derived C into the fungal communities (Fig. 5). Fungal hyphae promote the occlusion of oPOM within aggregated soil structures via the enmeshment of mineral particles (Dungait et al., 2012; Oades and Waters, 1991; Witzgall et al., 2021). Intriguingly, this effect was not followed by a proportional increase in ^{13}C enrichment since oPOM δ^{13}C

Table 5
δ^{13}C values, (‰), net rhizodeposition ^{13}C (μg of ^{13}C excess g^{-1} of soil), and the relative distribution of net rhizodeposition ^{13}C at the following SOM fractions: free-particulate organic matter (fPOM), occluded organic matter (oPOM), sand-sized organic matter (SSOM), mineral associated organic matter (MAOM), mineral-organic complexes (MOC) and short-range order (SRO) phases and residual (not extracted).

SOM fractions		δ^{13}C (‰)	Net rhizodeposition ^{13}C (μg of ^{13}C excess g^{-1} of soil)	Relative distribution[2] (%)
fPOM		−28.0 ± 0.1	0.04 ± 0.02	3.0 % ±1
oPOM		−27.8 ± 0.1	0.02 ± 0.01	2.8 % ±1
SSOM		−24.6 ± 0.1	0.00 ± 0.00	0.0 % ±0
MAOM	MOC[1]	–	0.05 ± 0.03	6.6 % ±5
	SRO[1]	–	0.14 ± 0.06	12.5 % ±5
	Residual	–	0.58 ± 0.11	57.2 % ±4
	Subtotal	−20.0 ± 0.5	0.77 ± 0.14	76.2 % ±3
Not found		–	0.18 ± 0.05	18.0 % ±3
Bulk soil		−20.4 ± 0.5	1.01 ± 0.20	100 %

Means ± SE (n = 4) are presented.
[1] δ^{13}C values of MOC and SRO were not measured directly, but the net rhizodeposition ^{13}C were calculated by the difference between the ^{13}C abundance after and before the extraction
[2] The relative distribution was calculated according to the unfractionated soil from the treatment with rhizodeposition

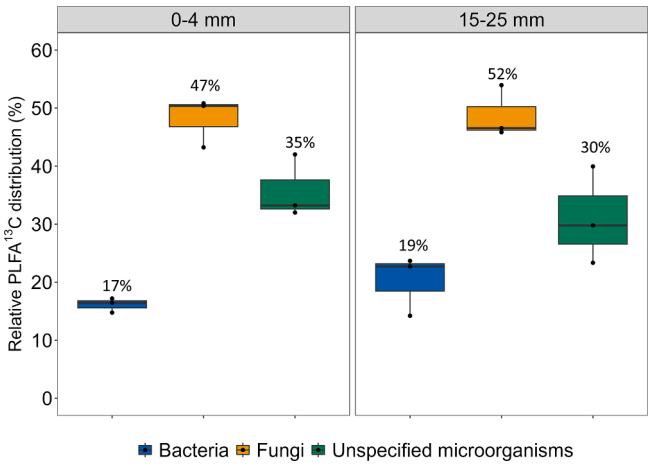

Fig. 5. Relative ^{13}C-labeled phospholipid fatty acids (^{13}C-PLFA) recovered from each microbial group. Means (n = 3) from the treatment with rhizodeposition are presented for the depths 0–4 and 15–25 mm.

values were only slightly changed from −28.1 ± 0.1 ‰ to −27.8 ± 0.1 ‰ (Table 2). One possible explanation for this result is that those organisms also fed on native SOM and not exclusively on rhizodeposits. Vidal et al. (2018) observed that bacterial cells in the rhizosphere were less enriched in ^{13}C than the roots themselves and concluded that this was a dilution effect caused by consuming "native" SOM.

We demonstrated that about 18 % of the net rhizodeposition ^{13}C amount was not recovered after the density-size fractionation procedure, despite having an excellent recovery of the total soil C (92 % of C recovery). The density fractionation procedure requires washing SPT excess from the fractions, which can promote the removal of soluble and weakly mineral-associated C (Plaza et al., 2019) such as net rhizodeposition ^{13}C (Marx et al., 2010; Neurath et al., 2021). In our results, we assume the non-recovered portion of net rhizodeposition ^{13}C is composed of this fraction. While this did not alter our main conclusions, we encourage future research to consider and report this C loss via density fractionation.

4.2. *Importance of reactive Al and Fe phases for the net rhizodeposition ^{13}C retention*

Our results show that more than one-fourth of the net rhizodeposition ^{13}C within the MAOM fraction was retained in the reactive Al and Fe phases (sum of MOC and SRO phases - Fig. 4). Meanwhile, most MAOM net rhizodeposition ^{13}C (75 %) was not extracted and remained in the residual MAOM fraction. These results reveal that the Al and Fe reactive phases have a sizeable importance for the retention of net rhizodeposition ^{13}C.

The extraction of SRO phases (hydroxylamine) yielded a higher amount of net rhizodeposition ^{13}C in relation to the MOC extraction (Na-pyrophosphate) (Fig. 4). Similar results were observed by Jeewani et al. (2020). SRO phases of Al and Fe are composed of poorly-crystalline minerals (e.g., allophane and ferrihydrite) with a high specific surface area and abundant hydroxyl reactive sites (Kramer et al., 2012). These minerals have a strong affinity for phenolic and carboxylic functional groups (Kramer et al., 2012; Mikutta et al., 2009; Scheel et al., 2008), which are both present in the root exudates of eucalypt plants (Andrade et al., 2022; Silva et al., 2004). These compounds have many reactive carboxyl groups, which can adsorb to these minerals or form precipitates that resist to microbial decomposition (Scheel et al., 2008, 2007; Strahm and Harrison, 2008).

MOC accounted for more than 40 % of the total C within the MAOM fraction, although had retained only 6.6 % of net rhizodeposition ^{13}C (Fig. 4 and Table 3). Large amounts of C associated with MOC have been previously observed in other studies, which suggests that this fraction comprises a sizeable soil C pool (Coward et al., 2017; Wagai et al., 2013). Nevertheless, the small retention of net rhizodeposition ^{13}C suggests that this fraction would be constituted predominantly by relatively older C pools, which is also corroborated by radiocarbon results (Heckman et al., 2018). Na-pyrophosphate extractions must always be interpreted cautiously, especially for tropical soils, due to problems with the non-selective extraction of Al-bearing minerals and to peptization and dispersal of Fe colloids (Rennert, 2019; Schuppli et al., 1983). It is not possible to ensure that our extracts were completely free of colloidal materials, which can lead to an overestimation of the C and the metal content associated with this fraction (Schuppli et al., 1983). Despite these issues, this extraction left more than 80 % of net rhizodeposition ^{13}C within the residual fraction (Fig. 4), which clearly indicates that net rhizodeposition ^{13}C was not majorly retained in this fraction.

Our results show that most net rhizodeposition ^{13}C was not extracted with the Al and Fe reactive phases and remained in the residual fraction (Fig. 4). This result implies that other minerals may be more critical for the retention of net rhizodeposition ^{13}C within the MAOM fraction. One possible mechanism could be the association of net rhizodeposition ^{13}C with more crystalline minerals, such as kaolinite and goethite, which are widespread in tropical soils (Schaefer, 2008). The retention of C in more crystalline phases is regarded as less effective due to the lower specific surface area and a reduced reactivity (Mikutta et al., 2006). However, other studies show that these minerals can still have an important role in protecting net rhizodeposition ^{13}C (Neurath et al., 2021).

Another possible mechanism is the protection of net rhizodeposition ^{13}C through the formation of stable microaggregates within the MAOM fraction (Lavallee et al., 2020; Totsche et al., 2018). Microaggregate formation is driven mainly by microbial-derived compounds, which act as a binding agent for the clay and silt-sized mineral particles (Oades and Waters, 1991). Our PLFA results show that rhizodeposition enhanced the abundance of microorganisms in the region close to the roots, which possibly contributed to the formation of these stable microaggregates (Table 4). Given the complex nature of the mineral-organic interactions (Kleber et al., 2021; Lehmann et al., 2020), it is likely that more than one mechanism operates for the retention of net rhizodeposition ^{13}C in the soil. Our study provides evidence that Al and Fe reactive phases are significant agents for the persistence of net rhizodeposition ^{13}C in the soil, but other underlying mechanisms are also likely to be involved.

4.3. *Net rhizodeposition spatial distribution and microbial community composition*

Our results showed that rhizodeposition increased the abundance of biomarkers of both fungal and bacterial communities in 0–4 mm layer but not at 15–25 mm from the roots (Table 4). These results reflect the distribution pattern of net rhizodeposition ^{13}C, which had its maximum closer to roots and decreased beyond the rhizoplane (Fig. 2). Soil microorganisms are limited mainly by C availability, and the input of easily decomposable organic substrates, such as the rhizodeposits, removes this limitation and boosts microbial activity (Kuzyakov and Blagodatskaya, 2015; Schimel and Weintraub, 2003). Since we observed a significant presence of net rhizodeposition ^{13}C at 15–25 mm, it was also expected to have enhanced microbial activity in this layer. Instead, our results suggest that the amount of net rhizodeposition ^{13}C dispersed through the 15–25 mm layer was insufficient to increase the microbial activity or change the microbial community structure composition. The effect of rhizodeposition on microbial activity is more limited, thus, to a relatively narrow zone of the soil, primarily close to the roots (Kuzyakov and Razavi, 2019).

The ^{13}C-PLFA distribution across the microbial biomarkers groups was very similar between the different layers (0–4 mm and 15–25 mm). About half of the ^{13}C-PLFA was incorporated into the fungal PLFAs (50 %), while bacterial biomarkers accounted only for about 19 % of the recovered ^{13}C-PLFA (Fig. 5). We expected that the high concentration of

C in the vicinity of the roots would result in a relatively higher ^{13}C enrichment in the bacterial PLFAs due to its higher capacity for processing soluble and easily-available substrates, which are major components of rhizodeposits (Gunina et al., 2014; Jones et al., 2009). Instead, our results indicate that fungi outcompete bacteria for the initial utilization of root exudates, which is also supported by several other studies (Ge et al., 2017; Yuan et al., 2017; Zhu et al., 2017). The dominance of fungi is attributed to their capacity for acquiring rhizodeposits through extended hyphal growth (Huang et al., 2020). Besides, the comparatively high proportion of fungal biomarkers in the 15–25 mm layer also suggests that these organisms are serving as a long-distance conduit for the transfer of plant-derived C from the rhizosphere to the bulk soil, as has also been previously observed by Vidal et al. (2021) for plant litter. Together, these results provide evidence for the importance of fungi not only as the major microbial group for the processing of rhizodeposits and formation of rhizodeposit-derived SOM but also as an active agent of dispersal of rhizodeposit C beyond the root vicinity.

5. Conclusions

We provide direct evidence that majority of net rhizodeposition was retained in soil as mineral-associated organic matter (MAOM) and, to a lower extent, as occluded POM. We found that 28 % of the net-rhizodeposition C within the MAOM fraction was retained in association with the Al and Fe reactive phases, indicating that this is a sizeable and important fraction for the retention of rhizodeposits in the soil. Additionally, we observed that rhizodeposition strongly increasedthe abundance of microbial PLFAs in the root vicinity (0–4 mm) but not in the more distant regions of the root-free compartments (15–25 mm). This indicates that the effects of rhizodeposition on microbial activity are spatially constrained to a (small) soil volume in the direct vicinity of the root. Based on the ^{13}C-PLFA results, we show that the fungal community was the microbial group that incorporated the higher proportion of rhizodeposits. We thus emphasize the role of fungi in transferring root-derived C beyond the root vicinity and promoting the formation of occluded POM.

CRediT authorship contribution statement

Pedro P.C. Teixeira: Conceptualization, Data curation, Formal analysis, Investigation, Methodology, Validation, Visualization, Writing – original draft, Writing – review & editing. **Alix Vidal:** Conceptualization, Funding acquisition, Supervision, Writing – original draft, Writing – review & editing, Investigation. **Ana P.M. Teixeira:** Conceptualization, Data curation, Formal analysis, Methodology, Visualization, Writing – original draft, Writing – review & editing. **Ivan F. Souza:** Conceptualization, Writing – original draft, Writing – review & editing. **Luís C.C. Hurtarte:** Conceptualization, Writing – original draft. **Danilo H.S. Silva:** Conceptualization, Formal analysis, Investigation, Methodology. **Luís F.J. Almeida:** Conceptualization, Formal analysis, Writing – original draft. **Franz Buegger:** Methodology, Writing – original draft. **Edith C. Hammer:** Methodology, Writing – original draft. **Jan Jansa:** Methodology, Writing – original draft. **Carsten W. Mueller:** Conceptualization, Formal analysis, Funding acquisition, Investigation, Supervision, Writing – original draft, Writing – review & editing. **Ivo R. Silva:** Conceptualization, Formal analysis, Funding acquisition, Investigation, Project administration, Supervision, Writing – original draft.

Declaration of competing interest

The authors declare that they have no known competing financial interests or personal relationships that could have appeared to influence the work reported in this paper.

Data availability

Data will be made available on request.

Acknowledgments

This study was financed by Conselho Nacional de Desenvolvimento Científico e Tecnológico (CNPq) and by Coordenação de Aperfeiçoamento de Pessoal de Nível Superior – Brasil (CAPES) – Finance Code 001. I.F.S received funding from the Coordenação de Aperfeiçoamento de Pessoal de Nível Superior (CAPES) as part of the Estágio Pós-Doutoral do Programa Nacional de Pós-Doutorado/Capes (PNPD/CAPES), grant number 88887.356500/2019-00". We acknowledge: Humberto Teixeira Rosado and João José de Miranda Milagres (Laboratório de Isótopos Estáveis – Universidade Federal de Viçosa) for their support with the ^{13}C plant labeling; Daniela C. Costa, Bernardo A. da Silva, Natal R. de Castro Júnior and Pedro C. Batista (Universidade Federal de Viçosa) for helping with the experiment sampling; Franziska Bucka and Kristina Witzgall (Technical University of Munich) for the help with PLFA extraction and with the calculations.

Appendix A. Supplementary data

Supplementary data to this article can be found online at https://doi.org/10.1016/j.geoderma.2024.116811.

References

Andrade, S.A.L., Borghi, A.A., De Oliveira, V.H., Gouveia, L.D.M., Martins, A.P.I., Mazzafera, P., 2022. Phosphorus shortage induces an increase in root exudation in fifteen eucalypts species. Agronomy 12, 2041. https://doi.org/10.3390/agronomy12092041.

Angst, G., Kögel-Knabner, I., Kirfel, K., Hertel, D., Mueller, C.W., 2016. Spatial distribution and chemical composition of soil organic matter fractions in rhizosphere and non-rhizosphere soil under European beech (Fagus sylvatica L.). Geoderma 264, 179–187. https://doi.org/10.1016/j.geoderma.2015.10.016.

Angst, G., Mueller, K.E., Kögel-Knabner, I., Freeman, K.H., Mueller, C.W., 2017. Aggregation controls the stability of lignin and lipids in clay-sized particulate and mineral associated organic matter. Biogeochemistry 132, 307–324. https://doi.org/10.1007/s10533-017-0304-2.

Angst, G., Mueller, K.E., Castellano, M.J., Vogel, C., Wiesmeier, M., Mueller, C.W., 2023. Unlocking complex soil systems as carbon sinks: multi-pool management as the key. Nat. Commun. 14, 2967. https://doi.org/10.1038/s41467-023-38700-5.

Baumert, V.L., Vasilyeva, N.A., Vladimirov, A.A., Meier, I.C., Kögel-Knabner, I., Mueller, C.W., 2018. Root exudates induce soil macroaggregation facilitated by fungi in subsoil. Front. Environ. Sci. 6 https://doi.org/10.3389/fenvs.2018.00140.

Baumert, V.L., Forstner, S.J., Zethof, J.H.T., Vogel, C., Heitkötter, J., Schulz, S., Kögel-Knabner, I., Mueller, C.W., 2021. Root-induced fungal growth triggers macroaggregation in forest subsoils. Soil Biol. Biochem. 157, 108244 https://doi.org/10.1016/j.soilbio.2021.108244.

Carolino de Sá, M.A., Lima, J.M., Silva, M.L.N., Dias Junior, M.S., 1999. Índice De Desagregação Do Solo Baseado Em Energia Ultra-Sônica. Rev. Bras. Ciênc. Solo 23, 525–531. https://doi.org/10.1590/s0100-06831999000300005.

Cotrufo, M.F., Wallenstein, M.D., Boot, C.M., Denef, K., Paul, E., 2013. The Microbial Efficiency-Matrix Stabilization (MEMS) framework integrates plant litter decomposition with soil organic matter stabilization: do labile plant inputs form stable soil organic matter? Glob. Change Biol. 19, 988–995. https://doi.org/10.1111/gcb.12113.

Coward, E.K., Thompson, A.T., Plante, A.F., 2017. Iron-mediated mineralogical control of organic matter accumulation in tropical soils. Geoderma 306, 206–216. https://doi.org/10.1016/j.geoderma.2017.07.026.

Dungait, J.A.J., Hopkins, D.W., Gregory, A.S., Whitmore, A.P., 2012. Soil organic matter turnover is governed by accessibility not recalcitrance. Glob. Change Biol. 18, 1781–1796. https://doi.org/10.1111/j.1365-2486.2012.02665.x.

Fox, J., Weisberg, S., 2019. An R Companion to Applied Regression. Sage, Thousand Oaks, USA.

Frostegård, Å., Tunlid, A., Bååth, E., 1991. Microbial biomass measured as total lipid phosphate in soils of different organic content. J. Microbiol. Methods 14, 151–163. https://doi.org/10.1016/0167-7012(91)90018-L.

Ge, T., Li, B., Zhu, Z., Hu, Y., Yuan, H., Dorodnikov, M., Jones, D.L., Wu, J., Kuzyakov, Y., 2017. Rice rhizodeposition and its utilization by microbial groups depends on N fertilization. Biol. Fertil. Soils 53, 37–48. https://doi.org/10.1007/s00374-016-1155-z.

Gunina, A., Dippold, M.A., Glaser, B., Kuzyakov, Y., 2014. Fate of low molecular weight organic substances in an arable soil: From microbial uptake to utilisation and stabilisation. Soil Biol. Biochem. 77, 304–313. https://doi.org/10.1016/j.soilbio.2014.06.029.

Hafner, S., Unteregelsbacher, S., Seeber, E., Lena, B., Xu, X., Li, X., Guggenberger, G., Miehe, G., Kuzyakov, Y., 2012. Effect of grazing on carbon stocks and assimilate partitioning in a Tibetan montane pasture revealed by $^{13}CO_2$ pulse labeling. Glob. Change Biol. 18, 528–538. https://doi.org/10.1111/j.1365-2486.2011.02557.x.

Heckman, K., Lawrence, C.R., Harden, J.W., 2018. A sequential selective dissolution method to quantify storage and stability of organic carbon associated with Al and Fe hydroxide phases. Geoderma 312, 24–35. https://doi.org/10.1016/j.geoderma.2017.09.043.

Hinsinger, P., Bengough, A.G., Vetterlein, D., Young, I.M., 2009. Rhizosphere: biophysics, biogeochemistry and ecological relevance. Plant Soil 321, 117–152. https://doi.org/10.1007/s11104-008-9885-9.

Huang, J., Liu, W., Deng, M., Wang, X., Wang, Z., Yang, L., Liu, L., 2020. Allocation and turnover of rhizodeposited carbon in different soil microbial groups. Soil Biol. Biochem. 150, 107973 https://doi.org/10.1016/j.soilbio.2020.107973.

Ingwersen, J., Poll, C., Streck, T., Kandeler, E., 2008. Micro-scale modelling of carbon turnover driven by microbial succession at a biogeochemical interface. Soil Biol. Biochem. 40, 864–878. https://doi.org/10.1016/j.soilbio.2007.10.018.

IUSS Working Group WRB, 2022. World Reference Base for Soil Resources. International Soil Classification System for Naming Soils and Creating Legends for Soil Maps, 4th edition. International Union of Soil Sciences (IUSS), Vienna, Austria.

Jeewani, P.H., Gunina, A., Tao, L., Zhu, Z., Kuzyakov, Y., Van Zwieten, L., Guggenberger, G., Shen, C., Yu, G., Singh, B.P., Pan, S., Luo, Y., Xu, J., 2020. Rusty sink of rhizodeposits and associated keystone microbiomes. Soil Biol. Biochem. 147, 107840 https://doi.org/10.1016/j.soilbio.2020.107840.

Johnson, D., Leake, J.R., Ostle, N., Ineson, P., Read, D.J., 2002. In situ 13CO2 pulse-labelling of upland grassland demonstrates a rapid pathway of carbon flux from arbuscular mycorrhizal mycelia to the soil. New Phytol. 153, 327–334. https://doi.org/10.1046/j.0028-646X.2001.00316.x.

Jones, D.L., Nguyen, C., Finlay, R.D., 2009. Carbon flow in the rhizosphere: Carbon trading at the soil-root interface. Plant Soil 321, 5–33. https://doi.org/10.1007/s11104-009-9925-0.

Kaiser, K., Guggenberger, G., 2003. Mineral surfaces and soil organic matter. Eur. J. Soil Sci. 54, 219–236. https://doi.org/10.1046/j.1365-2389.2003.00544.x.

Kleber, M., Mikutta, R., Torn, M.S., Jahn, R., 2005. Poorly crystalline mineral phases protect organic matter in acid subsoil horizons, 050912034650054 Eur. J. Soil Sci.. https://doi.org/10.1111/j.1365-2389.2005.00706.x.

Kleber, M., Eusterhues, K., Keiluweit, M., Mikutta, C., Mikutta, R., Nico, P.S., 2015. Mineral-Organic Associations: Formation, Properties, and Relevance in Soil Environments, Advances in Agronomy. Elsevier Ltd. https://doi.org/10.1016/bs.agron.2014.10.005.

Kleber, M., Bourg, I.C., Coward, E.K., Hansel, C.M., Myneni, S.C.B., Nunan, N., 2021. Dynamic interactions at the mineral–organic matter interface. Nat. Rev. Earth Environ. 2, 402–421. https://doi.org/10.1038/s43017-021-00162-y.

Kögel-Knabner, I., 2017. The macromolecular organic composition of plant and microbial residues as inputs to soil organic matter: Fourteen years on. Soil Biol. Biochem. 105, A3–A8. https://doi.org/10.1016/j.soilbio.2016.08.011.

Kramer, S., Marhan, S., Haslwimmer, H., Ruess, L., Kandeler, E., 2013. Temporal variation in surface and subsoil abundance and function of the soil microbial community in an arable soil. Soil Biol. Biochem. 61, 76–85. https://doi.org/10.1016/j.soilbio.2013.02.006.

Kramer, M.G., Sanderman, J., Chadwick, O.A., Chorover, J., Vitousek, P.M., 2012. Long-term carbon storage through retention of dissolved aromatic acids by reactive particles in soil. Glob. Change Biol. 18, 2594–2605. https://doi.org/10.1111/j.1365-2486.2012.02681.x.

Kuzyakov, Y., Blagodatskaya, E., 2015. Microbial hotspots and hot moments in soil: Concept & review. Soil Biol. Biochem. 83, 184–199. https://doi.org/10.1016/j.soilbio.2015.01.025.

Kuzyakov, Y., Razavi, B.S., 2019. Rhizosphere size and shape: Temporal dynamics and spatial stationarity. Soil Biol. Biochem. 135, 343–360. https://doi.org/10.1016/j.soilbio.2019.05.011.

Lavallee, J.M., Soong, J.L., Cotrufo, M.F., 2020. Conceptualizing soil organic matter into particulate and mineral-associated forms to address global change in the 21st century. Glob. Change Biol. 26, 261–273. https://doi.org/10.1111/gcb.14859.

Lehmann, J., Hansel, C.M., Kaiser, C., Kleber, M., Maher, K., Manzoni, S., Nunan, N., Reichstein, M., Schimel, J.P., Torn, M.S., Wieder, W.R., Kögel-Knabner, I., 2020. Persistence of soil organic carbon caused by functional complexity. Nat. Geosci. 13, 529–534. https://doi.org/10.1038/s41561-020-0612-3.

Machado, D.N., Novais, R.F., da Silva, I.R., Loureiro, M.E., Milagres, J.J., Soares, E.M.B., 2011. Enriquecimento e alocação de ^{13}C em plantas de eucalipto. Rev. Bras. Ciênc. Solo 35, 857–866. https://doi.org/10.1590/S0100-06832011000300020.

Marx, M., Buegger, F., Gattinger, A., Zsolnay, Á., Charles Munch, J., 2010. Determination of the fate of regularly applied 13C-labeled-artificial-exudates C in two agricultural soils. J. Plant Nutr. Soil Sci. 173, 80–87. https://doi.org/10.1002/jpln.200800104.

Mikutta, R., Kleber, M., Torn, M.S., Jahn, R., 2006. Stabilization of soil organic matter: Association with minerals or chemical recalcitrance? Biogeochemistry 77, 25–56. https://doi.org/10.1007/s10533-005-0712-6.

Mikutta, R., Schaumann, G.E., Gildemeister, D., Bonneville, S., Kramer, M.G., Chorover, J., Chadwick, O.A., Guggenberger, G., 2009. Biogeochemistry of mineral–organic associations across a long-term mineralogical soil gradient (0.3–4100kyr), Hawaiian Islands. Geochim. Cosmochim. Acta 73, 2034–2060. https://doi.org/10.1016/j.gca.2008.12.028.

Mikutta, R., Zang, U., Chorover, J., Haumaier, L., Kalbitz, K., 2011. Stabilization of extracellular polymeric substances (Bacillus subtilis) by adsorption to and coprecipitation with Al forms. Geochim. Cosmochim. Acta 75, 3135–3154. https://doi.org/10.1016/j.gca.2011.03.006.

Mikutta, R., Turner, S., Schippers, A., Gentsch, N., Meyer-Stüve, S., Condron, L.M., Peltzer, D.A., Richardson, S.J., Eger, A., Hempel, G., Kaiser, K., Klotzbücher, T., Guggenberger, G., 2019. Microbial and abiotic controls on mineral-associated organic matter in soil profiles along an ecosystem gradient. Sci. Rep. 9, 10294. https://doi.org/10.1038/s41598-019-46501-4.

Mueller, C.W., Koegel-Knabner, I., 2009. Soil organic carbon stocks, distribution, and composition affected by historic land use changes on adjacent sites. Biol. Fertil. Soils 45, 347–359. https://doi.org/10.1007/s00374-008-0336-9.

Neurath, R.A., Pett-Ridge, J., Chu-Jacoby, I., Herman, D., Whitman, T., Nico, P.S., Lipton, A.S., Kyle, J., Tfaily, M.M., Thompson, A., Firestone, M.K., 2021. Root carbon interaction with soil minerals is dynamic, leaving a legacy of microbially derived residues. acs.est.1c00300 Environ. Sci. Technol.. https://doi.org/10.1021/acs.est.1c00300.

Novais, R.F., Neves, J.C.L., Barros, N.F., 1991. Ensaio em ambiente controlado. In: de Oliveira, A.J., Garrido, W.E., de Araujo, J.D., Lourenço, S. (Eds.), Métodos De Pesquisa Em Fertilidade Do Solo. Embrapa, Brasilia, pp. 189–209.

Oades, J.M., Waters, A.G., 1991. Aggregate hierarchy in soils. Aust. J. Soil Res. 29, 815–825. https://doi.org/10.1071/SR9910815.

Paterson, E., Gebbing, T., Abel, C., Sim, A., Telfer, G., 2007. Rhizodeposition shapes rhizosphere microbial community structure in organic soil. New Phytol. 173, 600–610. https://doi.org/10.1111/j.1469-8137.2006.01931.x.

Pausch, J., Kuzyakov, Y., 2018. Carbon input by roots into the soil: Quantification of rhizodeposition from root to ecosystem scale. Glob. Change Biol. 24, 1–12. https://doi.org/10.1111/gcb.13850.

Plaza, C., Giannetta, B., Benavente, I., Vischetti, C., Zaccone, C., 2019. Density-based fractionation of soil organic matter: effects of heavy liquid and heavy fraction washing. Sci. Rep. 9, 10146. https://doi.org/10.1038/s41598-019-46577-y.

Poll, C., Ingwersen, J., Stemmer, M., Gerzabek, M.H., Kandeler, E., 2006. Mechanisms of solute transport affect small-scale abundance and function of soil microorganisms in the detritusphere. Eur. J. Soil Sci. 57, 583–595. https://doi.org/10.1111/j.1365-2389.2006.00835.x.

Porras, R.C., Hicks Pries, C.E., McFarlane, K.J., Hanson, P.J., Torn, M.S., 2017. Association with pedogenic iron and aluminum: effects on soil organic carbon storage and stability in four temperate forest soils. Biogeochemistry 133, 333–345. https://doi.org/10.1007/s10533-017-0337-6.

R Core Team, 2022. R: A Language and Environment for Statistical Computing.

Rennert, T., 2019. Wet-chemical extractions to characterise pedogenic Al and Fe species – a critical review. Soil Res. 57, 1. https://doi.org/10.1071/SR18299.

RStudio, 2023. RStudio: Integrated Development Environment for R.

Schaefer, C.E.G.R., 2008. Minerals in the clay fraction of Brazilian Latosols (Oxisols): a review. https://doi.org/10.1180/claymin.2008.043.1.11.

Scheel, T., Dörfler, C., Kalbitz, K., 2007. Precipitation of dissolved organic matter by aluminum stabilizes carbon in acidic forest soils. Soil Sci. Soc. Am. J. 71, 64–74. https://doi.org/10.2136/sssaj2006.0111.

Scheel, T., Haumaier, L., Ellerbrock, R.H., Rühlmann, J., Kalbitz, K., 2008. Properties of organic matter precipitated from acidic forest soil solutions. Org. Geochem. 39, 1439–1453. https://doi.org/10.1016/j.orggeochem.2008.06.007.

Schimel, J.P., Weintraub, M.N., 2003. The implications of exoenzyme activity on microbial carbon and nitrogen limitation in soil: A theoretical model. Soil Biol. Biochem. 35, 549–563. https://doi.org/10.1016/S0038-0717(03)00015-4.

Schuppli, P.A., Ross, G.J., McKeague, J.A., 1983. The effective removal of suspended materials from pyrophosphate extracts of soils from tropical and temperate regions. Soil Sci. Soc. Am. J. 47, 1026–1032. https://doi.org/10.2136/sssaj1983.03615995004700050037x.

Shahzad, T., Chenu, C., Genet, P., Barot, S., Perveen, N., Mougin, C., Fontaine, S., 2015. Contribution of exudates, arbuscular mycorrhizal fungi and litter depositions to the rhizosphere priming effect induced by grassland species. Soil Biol. Biochem. 80, 146–155. https://doi.org/10.1016/j.soilbio.2014.09.023.

Silva, I.R., Novais, R.F., Jham, G.N., Barros, N.F., Gebrim, F.O., Nunes, F.N., Neves, J.C.L., Leite, F.P., 2004. Responses of eucalypt species to aluminum: the possible involvement of low molecular weight organic acids in the Al tolerance mechanism. Tree Physiol. 24, 1267–1277. https://doi.org/10.1093/treephys/24.11.

Sokol, N.W., Bradford, M.A., 2019. Microbial formation of stable soil carbon is more efficient from belowground than aboveground input. Nature Geosci 12, 46–53. https://doi.org/10.1038/s41561-018-0258-6.

Sokol, N.W., Sanderman, J., Bradford, M.A., 2018. Pathways of mineral-associated soil organic matter formation: integrating the role of plant carbon source, chemistry, and point-of-entry. Glob. Change Biol. 1–13 https://doi.org/10.1111/gcb.14482.

Sokol, N.W., Whalen, E.D., Jilling, A., Kallenbach, C., Pett-Ridge, J., Georgiou, K., 2022. Global distribution, formation and fate of mineral-associated soil organic matter under a changing climate: A trait-based perspective. Funct. Ecol. 36, 1411–1429. https://doi.org/10.1111/1365-2435.14040.

Souza, I.F., Archanjo, B.S., Hurtarte, L.C.C., Oliveros, M.E., Gouvea, C.P., Lidizio, L.R., Achete, C.A., Schaefer, C.E.R., Silva, I.R., 2017. Al-/Fe-(hydr)oxides–organic carbon associations in Oxisols — From ecosystems to submicron scales. Catena 154, 63–72. https://doi.org/10.1016/j.catena.2017.02.017.

Strahm, B.D., Harrison, R.B., 2008. Controls on the sorption, desorption and mineralization of low-molecular-weight organic acids in variable-charge soils. Soil Sci. Soc. Am. J. 72, 1653–1664. https://doi.org/10.2136/sssaj2007.0318.

Totsche, K.U., Amelung, W., Gerzabek, M.H., Guggenberger, G., Klumpp, E., Knief, C., Lehndorff, E., Mikutta, R., Peth, S., Prechtel, A., Ray, N., Kögel-Knabner, I., 2018. Microaggregates in soils. J. Plant Nutr. Soil Sci. 181, 104–136. https://doi.org/10.1002/jpln.201600451.

Vidal, A., Hirte, J., Bender, S.F., Mayer, J., Gattinger, A., Höschen, C., Schädler, S., Iqbal, T.M., Mueller, C.W., 2018. Linking 3D soil structure and plant-microbe-soil

carbon transfer in the rhizosphere. Front. Environ. Sci. 6, 1–14. https://doi.org/10.3389/fenvs.2018.00009.

Vidal, A., Klöffel, T., Guigue, J., Angst, G., Steffens, M., Hoeschen, C., Mueller, C.W., 2021. Visualizing the transfer of organic matter from decaying plant residues to soil mineral surfaces controlled by microorganisms. Soil Biol. Biochem. 160, 108347 https://doi.org/10.1016/j.soilbio.2021.108347.

Villarino, S.H., Pinto, P., Jackson, R.B., Piñeiro, G., 2021. Plant rhizodeposition: A key factor for soil organic matter formation in stable fractions. Sci. Adv. 7, eabd3176. https://doi.org/10.1126/sciadv.abd3176.

von Lützow, M., Kögel-Knabner, I., Ekschmitt, K., Matzner, E., Guggenberger, G., Marschner, B., Flessa, H., 2006. Stabilization of organic matter in temperate soils: mechanisms and their relevance under different soil conditions - a review: Mechanisms for organic matter stabilization in soils. Eur. J. Soil Sci. 57, 426–445. https://doi.org/10.1111/j.1365-2389.2006.00809.x.

von Lützow, M., Kögel-Knabner, I., Ekschmitt, K., Flessa, H., Guggenberger, G., Matzner, E., Marschner, B., 2007. SOM fractionation methods: Relevance to functional pools and to stabilization mechanisms. Soil Biol. Biochem. 39, 2183–2207. https://doi.org/10.1016/j.soilbio.2007.03.007.

von Lützow, M., Kögel-Knabner, I., Ludwig, B., Matzner, E., Flessa, H., Ekschmitt, K., Guggenberger, G., Marschner, B., Kalbitz, K., 2008. Stabilization mechanisms of organic matter in four temperate soils: Development and application of a conceptual model. J. Plant Nutr. Soil Sci. 171, 111–124. https://doi.org/10.1002/jpln.200700047.

Wagai, R., Mayer, L.M., Kitayama, K., Shirato, Y., 2013. Association of organic matter with iron and aluminum across a range of soils determined via selective dissolution techniques coupled with dissolved nitrogen analysis. Biogeochemistry 112, 95–109. https://doi.org/10.1007/s10533-011-9652-5.

Wickham, H., Averick, M., Bryan, J., Chang, W., McGowan, L., François, R., Grolemund, G., Hayes, A., Henry, L., Hester, J., Kuhn, M., Pedersen, T., Miller, E., Bache, S., Müller, K., Ooms, J., Robinson, D., Seidel, D., Spinu, V., Takahashi, K., Vaughan, D., Wilke, C., Woo, K., Yutani, H., 2019. Welcome to the Tidyverse. J. Open Source Softw. 4, 1686. https://doi.org/10.21105/joss.01686.

Wickham, H., 2016. ggplot2: Elegant Graphics for Data Analysis, 2nd ed. 2016. ed, Use R! Springer International Publishing: Imprint: Springer, Cham. https://doi.org/10.1007/978-3-319-24277-4.

Witzgall, K., Vidal, A., Schubert, D.I., Höschen, C., Schweizer, S.A., Buegger, F., Pouteau, V., Chenu, C., Mueller, C.W., 2021. Particulate organic matter as a functional soil component for persistent soil organic carbon. Nat. Commun. 12, 4115. https://doi.org/10.1038/s41467-021-24192-8.

Wu, T., Ost, A.D., Audinot, J.-N., Wiesmeier, M., Wirtz, T., Buegger, F., Häusler, W., Höschen, C., Mueller, C.W., 2022. Association of fresh low-molecular-weight organic compounds with clay-sized mineral fraction in soils of different organic carbon loading. Geoderma 409, 115657. https://doi.org/10.1016/j.geoderma.2021.115657.

Yuan, Y., Zhao, W., Xiao, J., Zhang, Z., Qiao, M., Liu, Q., Yin, H., 2017. Exudate components exert different influences on microbially mediated C losses in simulated rhizosphere soils of a spruce plantation. Plant Soil 419, 127–140. https://doi.org/10.1007/s11104-017-3334-6.

Zhu, Z., Ge, T., Hu, Y., Zhou, P., Wang, T., Shibistova, O., Guggenberger, G., Su, Y., Wu, J., 2017. Fate of rice shoot and root residues, rhizodeposits, and microbial assimilated carbon in paddy soil - part 2: turnover and microbial utilization. Plant Soil 416, 243–257. https://doi.org/10.1007/s11104-017-3210-4.